

Generative Feature Training of Thin 2-Layer Networks

Johannes Hertrich

Université Paris Dauphine - PSL

johannes.hertrich@dauphine.psl.eu

Sebastian Neumayer

Technische Universität Chemnitz

sebastian.neumayer@math.tu-chemnitz.de

Reviewed on OpenReview: <https://openreview.net/forum?id=6oXNpKuBDK>

Abstract

We consider the approximation of functions by 2-layer neural networks with only a few hidden weights based on the squared loss and small datasets. Due to the highly non-convex energy landscape, gradient-based training often suffers from local minima. As a remedy, we initialize the hidden weights with samples from a learned proposal distribution, which we parameterize as a deep generative model. To train this model, we exploit the fact that with fixed hidden weights, the optimal output weights solve a linear equation. After learning the generative model, we refine a set of sampled weights with a gradient-based feature refinement in the latent space. Here, we also include a regularization scheme to counteract potential noise. Finally, we demonstrate the effectiveness of our approach by numerical examples.

1 Introduction

We investigate the approximation of real-valued functions $f: [0, 1]^d \rightarrow \mathbb{R}$ based on samples $(x_k, y_k)_{k=1}^M$, where $x_k \in [0, 1]^d$ are independently drawn from some distribution ν_{data} and $y_k \approx f(x_k)$ are possibly noisy observations of $f(x_k)$. To achieve this, we study parametric architectures $f_{w,b}: [0, 1]^d \rightarrow \mathbb{R}$ of the form

$$f_{w,b}(x) = \Re \left(\sum_{l=1}^N b_l \Phi(\langle w_l, x \rangle) \right), \quad (1)$$

where \Re denotes the real part, $\Phi: \mathbb{R} \rightarrow \mathbb{C}$ is a nonlinear function, and $w_1, \dots, w_N \in \mathbb{R}^d$ are the features with corresponding weights $b_1, \dots, b_N \in \mathbb{C}$. If the function Φ is real-valued, the model (1) simplifies to a standard 2-layer neural network architecture without \Re and with $b_1, \dots, b_N \in \mathbb{R}$. The more general model (1) also covers other frameworks such as random Fourier features (Rahimi & Recht, 2007). Since the Pareto principle suggests that most real-world systems are driven by a few low-complexity interactions, we are interested in representations (1) with only a few features w_l . Such an explicit restriction of N also mitigates overfitting, as seen in sparse neural networks, compressed sensing and feature selection.

For fixed Φ and N , we aim to find $(w, b) \in \mathbb{R}^{d,N} \times \mathbb{C}^N$ such that the $f_{w,b}$ from (1) approximates f well. From a theoretical perspective, we can obtain such (\hat{w}, \hat{b}) by minimizing the mean squared error (MSE), namely

$$(\hat{w}, \hat{b}) \in \arg \min_{w, b} \|f - f_{w,b}\|_{L^2(\nu_{\text{data}})}^2. \quad (2)$$

In practice, we do not have access to ν_{data} and f , but only to data points $(x_k, y_k)_{k=1}^M$, where x_k are iid samples from ν_{data} and y_k are noisy versions of $f(x_k)$. Hence, we replace (2) by the empirical risk minimization

$$(\hat{w}, \hat{b}) \in \arg \min_{w, b} \sum_{k=1}^M |y_k - f_{w,b}(x_k)|^2. \quad (3)$$

However, if M is small, minimizing (3) can lead to overfitting towards the training samples $(x_k, y_k)_{k=1}^M$ and poor generalization. To address this issue, we investigate the following principles.

- We use $f_{w,b}$ of the form (1) with small N . This amounts to the implicit assumption that f can be *sparingly* represented using (1). Unfortunately, under-parameterized networks ($N \ll M$) are difficult to train with conventional gradient-based algorithms (Boob et al., 2022; Holzmüller & Steinwart, 2022), see also Table 1. Hence, we require an alternative training strategy.
- Often, we have prior information about the regularity of f , i.e., that f is in some Banach space \mathcal{B} with a norm of the form

$$\|f\|_{\mathcal{B}}^p = \int_{[0,1]^d} \|Df(x)\|_q^p dx, \quad (4)$$

where D is some differential operator and $p, q \geq 1$. A common example within this framework is the space of bounded variation (Ambrosio et al., 2000), which informally corresponds to the choice $D = \nabla$, $q = 2$ and $p = 1$. In practice, the integral in (4) is often approximated using Monte Carlo methods with uniformly distributed samples $(\tilde{x}_m)_{m=1}^S \subset [0, 1]^d$. If we use (4) as regularizer for $f_{w,b}$, the generalization error can be analyzed in Barron spaces (Li et al., 2022).

Contribution We propose a generative modeling approach to solve (3). To this end, we first observe that the minimization with respect to b is a linear least squares problem. Hence, we can analytically express the optimal \hat{b} in terms of w , which leads to a reduced problem. Using the implicit function theorem, we compute $\nabla_w \hat{b}(w)$ and hence the gradient of the reduced objective. To facilitate its optimization, we replace the deterministic features w with stochastic ones, and optimize over their underlying distribution p_w instead. We parameterize this distribution as $p_w = G_{\theta\#}\mathcal{N}(0, I_d)$ with a deep network $G_{\theta}: \mathbb{R}^d \rightarrow \mathbb{R}^d$. Hence, we coin our approach as *generative feature training*. Further, we propose to add a Monte Carlo approximation of the norm (4) to the reduced objective. With this regularization, we aim to prevent overfitting.

2 Related Work

Random Features Random feature models (RFM) first appeared in the context of kernel approximation (Rahimi & Recht, 2007; Liu et al., 2021), which enables the fast computation of large kernel sums with certain error bounds, see also Rahimi & Recht (2008); Cortes et al. (2010); Rudi & Rosasco (2017). A similar strategy is pursued by Huang et al. (2006) under the name extreme learning machines. Sparse RFMs (Yen et al., 2014) of the form (1) with only a few active features can be computed based on ℓ_1 basis pursuit (Hashemi et al., 2023). Since this often leads to suboptimal approximation accuracy, later works by Xie et al. (2022); Saha et al. (2023); Bai et al. (2024) instead proposed to apply pruning or hard-thresholding algorithms to reduce the size of w . Commonly, the features w are sampled from Gaussian mixtures with diagonal covariances. Unlike our approach, all these methods begin with a large feature set that has to contain sufficiently many relevant ones. Towards this strong implicit assumption, Potts & Schmischke (2021); Potts & Weidensager (2025) propose to identify the relevant subspaces for the feature proposal based on the ANOVA decomposition. Unfortunately, this only works if the features w itself are sparse (few non-zero entries), see Figure 1. Sparse features also enable the fast evaluation of the $f_{w,b}$ from (1) via the non-equispaced fast Fourier transform (Dutt & Rokhlin, 1993; Potts et al., 2001). For kernel approximations, this can be also achieved with slicing methods (Hertrich, 2024; Hertrich et al., 2025), which are again closely related to RFMs (Rux et al., 2025).

Adaptive Features Besides our work, there are several attempts to design data-adapted proposal distributions p_w for random features (Li et al., 2019c; Dunbar et al., 2025). Recently, Bolager et al. (2023) proposed to sample the features w in regions where it matters, i.e., based on the available gradient information. While this allows some adaption, the w still remain fixed after sampling them (a so-called greedy approach). Towards fully adaptive (Fourier) features w , Li et al. (2019b) propose to alternately solve for the optimal b , and to then perform a gradient update for the w . Kammonen et al. (2020) propose to instead update the w based on a Markov Chain Monte Carlo method. Unlike our approach, both methods do not incorporate the gradient information of b into the update process of p_w . It is well known that the surrogate alternating updates may perform poorly in certain cases. Note that learnable features have been also used in the context of positional encoding (Li et al., 2021) and implicit kernel learning (Li et al., 2019a).

2-Layer ReLU Networks We can interpret 2-layer neural networks as adaptive kernel methods (E et al., 2019). Moreover, they have essentially the same generalization error as the RFM. Several works investigate the learning of the architecture (1) with $\Phi = \text{ReLU}$ based on a (modified) version of the empirical risk minimization (3). Based on convex duality, Pilanci & Ergen (2020) derive a semi-definite program to find a global minimizer of (3). A huge drawback is that this method scales exponentially in the dimension d . Later, several accelerations based on convex optimization algorithms have been proposed (Mishkin et al., 2022; Bai et al., 2023). Following a different approach, Barbu (2023) proposed to use an alternating minimization over the parameters w and b that keeps the activation pattern fixed throughout the training. While this has an improved complexity of $\mathcal{O}(d^3)$ in d , the approach is still restricted to ReLU-like functions Φ . Moreover, gradient-based optimization of the parameters for a generative (proposal) network such as ours is empirically known to scale very well with d . A discussion of the rich literature on global minimization guarantees in the over-parameterized regime ($N \gg M$) is not within the scope of a sparse architecture (1).

Bayesian Networks Another approach that samples neural network weights is Bayesian neural networks (BNNs) (Neal, 2012; Jospin et al., 2022). This allows to capture the uncertainty on the weights in over-parameterized architectures. A fundamental difference to our approach and RFMs is that we sample the features $(w_l)_{l=1}^N$ independently from the same distribution, while BNNs usually learn a separate one for each w_l . Further, BNNs are usually trained by minimizing an evidence lower bound instead of (8), see for example (Graves, 2011; Blundell et al., 2015), which is required to prevent collapsing distributions.

3 Generative Feature Learning

Given data points $(x_k, y_k)_{k=1}^M$ with $y_k \approx f(x_k)$ for some underlying $f: [0, 1]^d \rightarrow \mathbb{R}$, we aim to find the optimal features $w = (w_l)_{l=1}^N \subset \mathbb{R}^d$ and weights $b \in \mathbb{C}^N$ such that $f_{w,b} \approx f$, where $f_{w,b}$ is defined in (1). Before we give our approach, we discuss two important instances of the nonlinearity $\Phi: \mathbb{R} \rightarrow \mathbb{C}$ from the literature.

- **Fourier Features:** The choice $\Phi(x) = e^{2\pi i x}$ is reasonable if the ground-truth function f can be represented by few Fourier features, e.g., if it is smooth. As discussed in Section 2, the deployed features w are commonly selected by randomized pruning algorithms.
- **2-Layer Neural Network:** For $\Phi: \mathbb{R} \rightarrow \mathbb{R}$, we can restrict ourselves to $b \in \mathbb{R}^N$. Common examples are the ReLU $\Phi(x) = \max(x, 0)$ and the sigmoid $\Phi(x) = \frac{e^x}{1+e^x}$. Then, $f_{w,b}$ corresponds to a 2-layer neural network (i.e., with one hidden layer). Using the so-called bias trick, we can include a bias into (1). That is, we use padded data-points $(x_k, 1) \in \mathbb{R}^{d+1}$ such that the last entry of the feature vectors $w_l \in \mathbb{R}^{d+1}$ can act as bias. Similarly, an output bias can be included.

In the following, we outline our procedure for optimizing the parameters w and b for a general $f_{w,b}$ of the form (1). First, we derive an analytic formula for the optimal weights b in the empirical risk minimization (3) with fixed features w . Then, in the spirit of random Fourier features, we propose to sample the w from a proposal distribution p_w , which we learn based on the generative modeling ansatz $p_w = G_{\theta\#}\mathcal{N}(0, I_d)$. As last step, we fine-tune the sampled features $w = G_{\theta}(z)$ by updating a set of sampled latent features z with the Adam optimizer. In order to be able to deal with noisy function values $y_k \approx f(x_k)$, we can regularize the approximation $f_{w,b}$ during training. Our complete approach is summarized in Algorithm 1.

3.1 Computing the Optimal Weights

For fixed $w = (w_l)_{l=1}^N$, any optimal weights $b(w) \in \mathbb{C}^N$ for (3) solve the linear system

$$A_w^T A_w b(w) = A_w^T y, \quad (5)$$

where $y = (y_k)_{k=1}^M$ and $A_w = (\Phi(\langle x_k, w_l \rangle))_{k,l=1}^{N,M}$. In order to stabilize the numerical solution of (5), we deploy Tikhonov regularization with small regularization strength $\varepsilon > 0$. This resolves the potential rank deficiency of $A_w^T A_w$ and we compute $b(w)$ as the unique solution of

$$(A_w^T A_w + \varepsilon I) b(w) = A_w^T y. \quad (6)$$

Algorithm 1 GFT and GFT-r training procedures.

```

1: Given: data  $(x_k, y_k)_{k=1}^M$ , architecture  $f_{w,b}$  as in (1), generator  $G_\theta$ , latent distribution  $\eta$ 
2: while training  $G_\theta$  do
3:   sample  $N$  latent  $z_l \sim \eta$  and set  $w = G_\theta(z)$ 
4:   compute optimal  $b(w)$  and  $\nabla_w b(w)$  based on (6)
5:   compute  $\nabla_\theta \mathcal{L}(\theta)$  or  $\nabla_\theta \mathcal{L}_{\text{reg}}(\theta)$  with automatic differentiation
6:   perform Adam update for  $\theta$ 
7: if GFT-r then
8:   while refining  $w$  do
9:     set  $w = G_\theta(z)$ 
10:    compute optimal  $b(w)$  and  $\nabla_w b(w)$  based on (6)
11:    compute  $\nabla_z F(z)$  or  $\nabla_z F_{\text{reg}}(z)$  with automatic differentiation
12:    perform Adam update for  $z$ 
13: Output: features  $w$  and optimal weights  $b(w)$ 

```

For $\epsilon \rightarrow 0$, the solution of (6) converges to the minimal norm solution of (5). A key aspect of our approach is that we can compute $\nabla_w b(w)$ using the implicit function theorem. This requires solving a linear equation of the form (6) with a different right hand side. For small N , the most efficient approach for solving (6) is to use a LU decomposition, and to reuse the decomposition for the backward pass. This procedure is implemented in many automatic differentiation packages such as PyTorch, and no additional coding is required.

By inserting the solution $b(w)$ of (6) into the empirical loss (3), we obtain the reduced loss

$$L(w) = \sum_{k=1}^M |f(x_k) - f_{w,b(w)}(x_k)|^2. \quad (7)$$

Naively, we can try to minimize (7) directly via a gradient-based method (such as Adam with its default parameters) starting at some random initialization $w^0 = (w_l^0)_{l=1}^N \subset \mathbb{R}^d$. We refer to this as feature optimization (F-Opt). However, $L(w)$ is non-convex, and our comparisons in Section 4 reveal that feature optimization frequently gets stuck in local minima. Consequently, a good initialization w^0 is crucial if we want to minimize (7) with a gradient-based method. In the spirit of random Fourier features, we propose to initialize the w as independent identically distributed (iid) samples from a proposal distribution p_w . To the best of our knowledge, current random Fourier feature methods all rely on a handcrafted p_w .

3.2 Learning the Proposal Distribution

Since the optimal p_w is in general not expressible without knowledge of f , we aim to learn it from the available data $(x_k, y_k)_{k=1}^M$ based on a generative model. That is, we take a simple latent distribution η (such as the normal distribution $\mathcal{N}(0, I_d)$) and make the parametric ansatz $p_w = G_\theta \# \eta$. Here, $G_\theta: \mathbb{R}^d \rightarrow \mathbb{R}^d$ is a fully connected neural network with parameters θ and $\#$ denotes the push-forward of η under G_θ . To optimize the parameters θ of the distribution $p_w = G_\theta \# \eta$, we minimize the expectation of the reduced loss (7) with iid features sampled from $G_\theta \# \eta$, namely the loss

$$\mathcal{L}(\theta) = \mathbb{E}_{w \sim (G_\theta \# \eta)^{\otimes N}} [L(w)] = \mathbb{E}_{z \sim \eta^{\otimes N}} [L(G_\theta(z))] = \mathbb{E}_{z \sim \eta^{\otimes N}} \left[\sum_{k=1}^M |f(x_k) - f_{G_\theta(z), b(G_\theta(z))}(x_k)|^2 \right], \quad (8)$$

where the notation $\mu^{\otimes N}$ denotes N -times the product measure of μ . We minimize the loss (8) by a stochastic gradient-based algorithm. That is, in each step, we sample one realization $z \sim \eta^{\otimes N}$ of the latent features to get an estimate for the expectation in (8). Then, we compute the gradient of the integrand with respect to θ for this specific z , and update θ with our chosen optimizer. In the following, we provide some intuition why this outperforms standard training approaches. In the early training phase, most of the sampled features w do not fit to the data. Hence, they suffer from vanishing gradients and are updated only slowly. On the other hand, since the stochastic generator $G_\theta \# \eta$ leads to an evaluation of the objective $L(w)$ at many different

locations, we quickly gather gradient information for a large variety of features. In particular, always taking fresh samples from the iteratively updated proposal distribution p_w helps to get rid of useless features.

3.3 Feature Refinement: Adam in the Latent Space

Once the feature distribution $p_w = G_\theta \# \eta$ is learned, we sample a collection $z^0 = (z_l^0)_{l=1}^N$ of iid latent features $z_l^0 \sim \eta$. By design, the associated features $w^0 = G_\theta(z^0)$ (with G_θ being applied elementwise to z_1^0, \dots, z_N^0) serve as an estimate for a minimizer of (7). Since these w^0 are only an estimate, we refine them similarly as described for the plain feature optimization approach from Section 3.1. More precisely, starting in z^0 instead of a random initialization, we minimize the function

$$F(z) = L(G_\theta(z)) = \sum_{k=1}^M |f(x_k) - f_{G_\theta(z), b(G_\theta(z))}(x_k)|^2, \quad (9)$$

where L is the loss function from (7). By noting that $\nabla F(z) = \nabla G_\theta(z)^\top \nabla L(G_\theta(z))$, this corresponds to initializing the Adam optimizer for the function $L(w)$ with $w^0 = G_\theta(z^0)$, and to additionally precondition it by the Jacobian matrix of the generator G_θ . If the step size is chosen appropriately, we expect that the value of $F(z)$ decreases with the iterations. Conceptually, our refinement approach is similar to many second-order optimization routines, which also require a good initialization for convergence.

3.4 Regularization for Noisy Data

If the number of training points M is small or if the noise on the $y_k \approx f(x_k)$ is strong, minimizing the empirical risk (3) can suffer from overfitting (i.e., the usage of high-frequency features). To prevent this, we deploy a regularizer of the form (4). Choosing $p = q = 1$ and $D = \nabla$ in (4) leads to the following training problem with (anisotropic) total variation regularization (Acar & Vogel, 1994; Chan & Esedoglu, 2005)

$$\hat{w} \in \arg \min_w \sum_{k=1}^M |y_k - f_{w, b(w)}(x_k)|^2 + \lambda R(w), \quad R(w) := \int_{[a_{\min}, a_{\max}]} \|\nabla f_{w, b(w)}(x)\|_1 \mathrm{d}x, \quad (10)$$

where $\lambda > 0$, and $a_{\min} = \min\{x_k : k = 1, \dots, M\}$ and $a_{\max} = \max\{x_k : k = 1, \dots, M\}$ are the entry-wise minimum and maximum of the training data. For our generative training loss (8), adding the regularizer from (10) leads to

$$\mathcal{L}_{\text{reg}}(\theta) = \mathbb{E}_{w \sim (G_\theta \# \eta)^{\otimes N}} [L(w) + \lambda R(w)]. \quad (11)$$

Similarly, we replace the F from (9) for the feature refinement in the latent space by

$$F_{\text{reg}}(z) = F(z) + \lambda R(G_\theta(z)). \quad (12)$$

If we have specific knowledge about the function f that we intend to approximate, then we can apply more restrictive regularizers of the form (10). As discussed in Section 2, several RFMs instead regularize the feature selection by enforcing that the features $w_l \in \mathbb{R}^d$ only have a few non-zero entries (sparse features).

Remark 1. *Given the nature of our numerical examples, we only discussed $f: [0, 1]^d \rightarrow \mathbb{R}$ with data points $y_k \in \mathbb{R}$. The extension of our method to multivariate $f: [0, 1]^d \rightarrow \mathbb{R}^n$ is straight forward.*

4 Experiments

We demonstrate the effectiveness of our method with three numerical examples. First, we visually inspect the obtained features. Here, we also check if they recover the correct subspaces. Secondly, we benchmark our methods on common test functions from approximation theory, i.e., with a known groundtruth. Lastly, we target regression on some datasets from the UCI database (Kelly et al., 2023).

4.1 Setup and Comparisons

For all our experiments, we set up the architecture f_w, b in (1) with $N = 100$ features $(w_l)_{l=1}^N$ and one of the nonlinearities Φ introduced in Section 3:

- We deploy $\Phi(x) = e^{2\pi i x}$ without the bias trick. This corresponds to the approximation of the underlying ground truth function by Fourier features.
- We deploy $\Phi(x) = \frac{e^x}{1+e^x}$, which corresponds to a 2-layer network with sigmoid activation functions. To improve the expressiveness of the model, we apply the bias trick for both layers.

An ablation for different choices of N is given in Appendix A. Further, we choose the generator G_θ for the proposal distribution $p_w = G_\theta \# \mathcal{N}(0, I_d)$ as ReLU network with 3 hidden layers and 512 neurons per hidden layer. To pick the regularization strength λ , we divide the original training data into a training (90%) and a validation (10%) set. Then, we train G_θ for each $\lambda \in \{0\} \cup \{1 \times 10^k : k = -4, \dots, 0\}$ and choose the λ with the best validation error. To minimize the regularized loss functions \mathcal{L}_{reg} (GFT, see also (11)) and F_{reg} (GFT-r, see also (12)), we run 40000 steps of the Adam optimizer. The remaining hyperparameters are given in Appendix C. We benchmark all our methods from Section 3.

- **F-Opt:** In the feature optimization, we minimize the $L(w)$ from (7) with a gradient-based optimizer starting with features w drawn from a standard normal distribution. As explained in Section 3.1, we expect that the optimization gets stuck in a local minimum. We verify this claim in our experiments.
- **GFT:** For the generative feature training as proposed in Section 3.2, we minimize the loss $\mathcal{L}(\theta)$ from (8) and draw iid features w from the generator G_θ during evaluation.
- **GFT-r:** For the refined generative feature training, we generate features using GFT and refine them with the procedure from Section 3.3. This requires to minimize the loss $F(z)$ in (9).

For each method, we specify the choice of Φ as ‘‘Fourier’’ and ‘‘sigmoid’’ activation in the corresponding tables. We compare the obtained results with algorithms from the random Fourier feature literature, and with standard training of neural networks. More precisely, we consider the following comparisons:

- **Sparse Fourier Features:** We compare with the random Fourier feature based methods SHRIMP (Xie et al., 2022), HARFE (Saha et al., 2023), SALSA (Kandasamy & Yu, 2016) and ANOVA-boosted random Fourier features (ANOVA-RFF; Potts & Weidensager, 2025). We do not rerun the methods and take the results reported by Xie et al. (2022); Potts & Weidensager (2025).
- **2-Layer Neural Networks:** We train the parameters of the 2-layer neural networks f_w, b with the Adam optimizer. Here, we use exactly the same architecture, loss function and activation function as for GFT. Additionally, we include results for the ReLU activation function $\Phi(x) = \max(x, 0)$.
- **Kernel Ridge Regression:** We perform a kernel ridge regression (Cristianini & Shawe-Taylor, 2000) with the Gaussian kernel, where the kernel parameter is chosen by the median rule.

Our PyTorch implementation is available online¹. We run all experiments on a NVIDIA RTX 4090 GPU. Depending on the specific model, the training takes between 30 seconds and 2 minutes. We include further ablations in Appendix B.

4.2 Visualization of Generated Features

First, we inspect the learned features w in a simple setting. To this end, we consider the function $g: \mathbb{R}^2 \rightarrow \mathbb{R}$ with $g(x) = \sin(4\pi x_1^2 + 1) + \cos(4\pi(x_2^4 + x_2))$. Since each summand of g depends either on x_1 or x_2 , its Fourier

¹available at https://github.com/johertrich/generative_feature_training

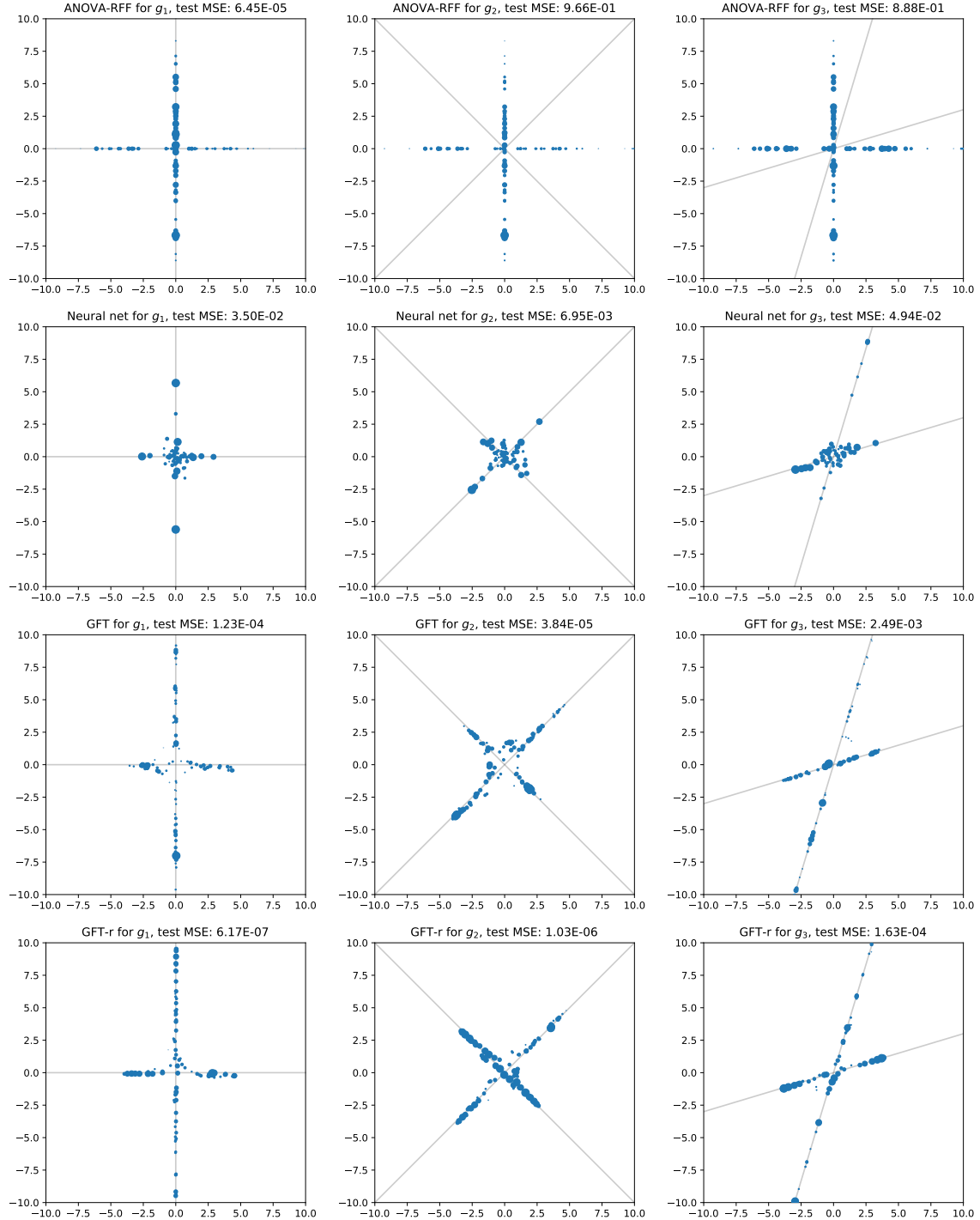


Figure 1: Location of the generated features for the g_i from (13), where the marker size reflects the magnitude of the associated weights b_l . The gray lines indicate the support of the Fourier transform of g_i . Since ANOVA-RFF constrains the features to be on the axes, it only works for g_1 . For the standard neural network training, the features are not pushed to the axis. This indicates that the optimization got stuck in a local minimum.

transform is supported on the coordinate axes. To make the task more challenging, we slightly adapt the problem by concatenating g with two linear transforms A_i , which leads to the three test functions

$$g_i(x) = g(A_i x), \quad \text{with} \quad A_1 = \begin{pmatrix} 1 & 0 \\ 0 & 1 \end{pmatrix}, \quad A_2 = \begin{pmatrix} \cos(\frac{\pi}{4}) & -\sin(\frac{\pi}{4}) \\ \sin(\frac{\pi}{4}) & \cos(\frac{\pi}{4}) \end{pmatrix}, \quad A_3 = \begin{pmatrix} 1 & 0.3 \\ 0.3 & 1 \end{pmatrix}. \quad (13)$$

In all cases, the Fourier transform is supported on a union of two subspaces. Now, we learn the features w with our GFT and GFT-r method based on 2000 samples that are drawn uniformly from $[0, 1]^2$, and plot them in Figure 1. The gray lines indicate the support of the Fourier transforms of g_i , and the size of the markers indicates the magnitude of the associated b_i . For all functions g_i , the features w sampled with GFT are mostly located in the support of the Fourier transform. The very few features that are located outside of it can be explained by numerical errors and are mostly removed by the refinement procedure GFT-r. In contrast, for ANOVA-RFF, the w are restricted to be located on the axes. Consequently, it cannot work for g_2 and g_3 , and the error obtained is large. For gradient-based neural network training, the w are not pushed to the axis, indicating that the optimization got stuck at a local minimum. For functions where the subspaces are orthogonal, such as g_2 , this issue was recently addressed in Ba et al. (2024) by learning the associated transform in the feature space.

4.3 Function Approximation

We use the same experimental setup as in (Potts & Weidensager, 2025, Table 7.1), that is, the test functions

- Polynomial: $f_1(x) = x_4^2 + x_2 x_3 + x_1 x_2 + x_4$;
- Isigami: $f_2(x) = \sin(x_1) + 7 \sin^2(x_2) + 0.1 x_3^4 \sin(x_1)$;
- Friedmann-1: $f_3(x) = 10 \sin(\pi x_1 x_2) + 20(x_3 - \frac{1}{2})^2 + 10x_4 + 5x_5$.

The input dimension d is set to 5 or 10 for each f_k . In particular, the f_k might not depend on all entries of the input x . For their approximation, we are given samples $x_k \sim \mathcal{U}_{[0,1]^d}$, $k = 1, \dots, M$, and the corresponding noise-less function values $f_k(x_k)$. The number of samples M and the dimension d are specified for each setting. As test set we draw M additional samples from $\mathcal{U}_{[0,1]^d}$. We deploy our methods as well as standard neural network training to the architecture $f_{w,b}$. The MSEs on the test set are given in Table 1. There, we also include ANOVA-random Fourier features, SHRIMP and HARFE for comparison. We always report the MSE for the best choice of ρ from Potts & Weidensager, 2025, Table 7.1. The GFT-r with Fourier activation functions outperforms the other approaches significantly. In particular, both the GFT and GFT-r consistently improve over the gradient-based training of the architecture $f_{w,b}$. This is in line with the analysis of gradient-based training in recent works (Boob et al., 2022; Holzmüller & Steinwart, 2022). As expected, Fourier activation functions are best suited for this task.

So far, we considered functions f_i that can be represented as sums, where each summand only depends on a small number of inputs x_i . While this assumption is crucial for the sparse Fourier feature methods from Table 1, it is not required for our methods. Therefore, we also benchmark them on the following non-decomposable functions and compare the results with standard gradient-based neural network training:

- $h_1(x) = \sin(\sum_{i=1}^d x_i) + \|x\|_2^2$
- $h_2(x) = \sqrt{\|x - \frac{1}{2}e\|_1}$, where e is the vector with all entries equal to one
- $h_3(x) = \sqrt{f_3(x)} = \sqrt{10 \sin(\pi x_1 x_2) + 20(x_3 - \frac{1}{2})^2 + 10x_4 + 5x_5}$.

The results are given in Table 2. As in the previous case, we can see a clear advantage of GFT and GFT-r.

Table 1: Comparison with sparse feature methods for function approximation: We report the MSE over the test set averaged over 5 runs. The values for ANOVA-RFF, SHRIMP and HARFE are taken from Potts & Weidensager (2025). The deployed λ is indicated below each result. The best performance is highlighted.

Method		Function f_1		Function f_2		Function f_3	
Method	Activation	$(d, M) = (5, 300)$	$(d, M) = (10, 500)$	$(d, M) = (5, 500)$	$(d, M) = (10, 1000)$	$(d, M) = (5, 500)$	$(d, M) = (10, 200)$
ANOVA-RFF	Fourier	1.40×10^{-6}	1.46×10^{-6}	2.65×10^{-5}	2.62×10^{-5}	1.00×10^{-4}	9.80×10^{-3}
SHRIMP	Fourier	1.83×10^{-6}	5.00×10^{-4}	8.20×10^{-3}	5.50×10^{-3}	2.00×10^{-4}	3.81×10^{-1}
HARFE	Fourier	5.82×10^{-1}	2.38×10^0	1.38×10^{-1}	6.65×10^{-1}	3.64×10^0	3.98×10^0
kernel ridge reg		5.90×10^{-5}	4.40×10^{-4}	7.1×10^{-5}	5.10×10^{-4}	1.15×10^{-2}	1.69×10^0
	Fourier	2.36×10^{-4} ($\lambda = 0$)	1.03×10^{-3} ($\lambda = 1 \times 10^{-4}$)	5.28×10^{-5} ($\lambda = 0$)	2.23×10^{-4} ($\lambda = 1 \times 10^{-4}$)	3.14×10^{-3} ($\lambda = 1 \times 10^{-4}$)	2.96×10^0 ($\lambda = 1 \times 10^{-4}$)
neural net	sigmoid	3.84×10^{-5} ($\lambda = 0$)	5.34×10^{-5} ($\lambda = 1 \times 10^{-4}$)	2.25×10^{-5} ($\lambda = 1 \times 10^{-4}$)	3.71×10^{-5} ($\lambda = 1 \times 10^{-4}$)	2.56×10^{-3} ($\lambda = 0$)	2.15×10^0 ($\lambda = 1 \times 10^{-3}$)
	ReLU	4.57×10^{-4} ($\lambda = 1 \times 10^{-4}$)	1.25×10^{-3} ($\lambda = 0$)	1.21×10^{-4} ($\lambda = 0$)	1.65×10^{-4} ($\lambda = 0$)	6.77×10^{-2} ($\lambda = 1 \times 10^{-4}$)	1.55×10^0 ($\lambda = 1 \times 10^{-3}$)
F-Opt	Fourier	2.50×10^{-3} ($\lambda = 1 \times 10^{-4}$)	1.08×10^0 ($\lambda = 1 \times 10^{-3}$)	2.36×10^{-6} ($\lambda = 1 \times 10^{-4}$)	1.31×10^0 ($\lambda = 1 \times 10^{-1}$)	5.93×10^{-2} ($\lambda = 0$)	1.68×10^1 ($\lambda = 1 \times 10^{-4}$)
	sigmoid	1.15×10^{-6} ($\lambda = 0$)	2.77×10^{-4} ($\lambda = 0$)	1.43×10^{-6} ($\lambda = 0$)	9.54×10^{-6} ($\lambda = 0$)	5.45×10^{-4} ($\lambda = 0$)	2.91×10^0 ($\lambda = 0$)
GFT	Fourier	2.72×10^{-7} ($\lambda = 0$)	5.00×10^{-7} ($\lambda = 0$)	1.03×10^{-7} ($\lambda = 0$)	4.09×10^{-7} ($\lambda = 0$)	5.87×10^{-5} ($\lambda = 1 \times 10^{-4}$)	4.47×10^{-3} ($\lambda = 1 \times 10^{-4}$)
	sigmoid	3.18×10^{-6} ($\lambda = 0$)	1.81×10^{-6} ($\lambda = 0$)	4.09×10^{-7} ($\lambda = 0$)	6.01×10^{-7} ($\lambda = 0$)	6.40×10^{-4} ($\lambda = 0$)	1.18×10^{-2} ($\lambda = 1 \times 10^{-4}$)
GFT-r	Fourier	6.05×10^{-8} ($\lambda = 0$)	5.46×10^{-8} ($\lambda = 0$)	2.02×10^{-8} ($\lambda = 0$)	8.15×10^{-8} ($\lambda = 0$)	6.26×10^{-6} ($\lambda = 0$)	1.89×10^{-4} ($\lambda = 0$)
	sigmoid	1.05×10^{-6} ($\lambda = 0$)	5.60×10^{-7} ($\lambda = 0$)	4.97×10^{-8} ($\lambda = 0$)	1.12×10^{-7} ($\lambda = 0$)	1.50×10^{-5} ($\lambda = 0$)	9.94×10^{-3} ($\lambda = 1 \times 10^{-4}$)

Table 2: Function approximation: We report the MSE over the test set averaged over 5 runs. The deployed λ is indicated below each result. The best performance is highlighted.

Method		Function h_1	Function h_2	Function h_3
Method	Activation	$(d, M) = (10, 1000)$	$(d, M) = (20, 1000)$	$(d, M) = (5, 500)$
kernel ridge reg		8.91×10^{-2}	3.74×10^{-3}	5.55×10^{-3}
	Fourier	6.03×10^{-2} ($\lambda = 1 \times 10^{-3}$)	1.34×10^{-2} ($\lambda = 0$)	2.68×10^{-4} ($\lambda = 0$)
neural net	sigmoid	4.17×10^{-2} ($\lambda = 0$)	5.94×10^{-3} ($\lambda = 1 \times 10^{-4}$)	4.42×10^{-4} ($\lambda = 1 \times 10^{-4}$)
	ReLU	5.64×10^{-1} ($\lambda = 1 \times 10^{-4}$)	6.89×10^{-3} ($\lambda = 1 \times 10^{-4}$)	5.56×10^{-3} ($\lambda = 1 \times 10^{-3}$)
F-Opt	Fourier	4.27×10^1 ($\lambda = 1 \times 10^0$)	5.06×10^0 ($\lambda = 1 \times 10^{-4}$)	7.24×10^{-3} ($\lambda = 1 \times 10^{-3}$)
	sigmoid	6.43×10^{-2} ($\lambda = 0$)	7.08×10^{-3} ($\lambda = 0$)	2.35×10^{-4} ($\lambda = 0$)
GFT	Fourier	2.62×10^{-2} ($\lambda = 1 \times 10^{-3}$)	3.54×10^{-3} ($\lambda = 1 \times 10^{-4}$)	2.34×10^{-4} ($\lambda = 1 \times 10^{-4}$)
	sigmoid	9.36×10^{-2} ($\lambda = 1 \times 10^{-4}$)	1.10×10^{-2} ($\lambda = 1 \times 10^{-4}$)	4.70×10^{-4} ($\lambda = 1 \times 10^{-4}$)
GFT-r	Fourier	8.96×10^{-3} ($\lambda = 0$)	2.57×10^{-3} ($\lambda = 1 \times 10^{-4}$)	1.04×10^{-4} ($\lambda = 0$)
	sigmoid	6.06×10^{-2} ($\lambda = 1 \times 10^{-3}$)	1.00×10^{-2} ($\lambda = 1 \times 10^{-4}$)	2.84×10^{-4} ($\lambda = 1 \times 10^{-4}$)

4.4 Regression on UCI Datasets

Next, we apply our method for regression on several UCI datasets Kelly et al. (2023). For this, we do not have an underlying ground truth function f . Here, we compare our methods with standard gradient-based neural network training, SHRIMP and SALSA. To this end, we use the numerical setup of SHRIMP. For each dataset, the MSE on the test split is given in Table 3. Compared to the other methods, SHRIMP and SALSA appear a bit more robust to noise and outliers, which frequently occur in the UCI datasets. This behavior is not surprising, since the enforced sparsity of the features w_l for those methods is a strong

Table 3: Regression on UCI datasets: We report the MSE on the test datasets averaged over 5 runs. The values for SHRIMP and SALSA are taken from Xie et al. (2022). The deployed λ is indicated below each result. The best performance is highlighted.

Method		Dataset					
Method	Activation	Propulsion (d, M) = (15, 200)	Galaxy (d, M) = (20, 2000)	Airfoil (d, M) = (41, 750)	CCPP (d, M) = (59, 2000)	Telemonit (d, M) = (19, 1000)	Skillkraft (d, M) = (18, 1700)
SHRIMP	Fourier	1.02×10^{-6}	5.41×10^{-6}	2.65×10^{-1}	6.55×10^{-2}	6.00×10^{-2}	5.81×10^{-1}
	Fourier	8.81×10^{-3}	1.35×10^{-4}	5.18×10^{-1}	6.78×10^{-2}	3.47×10^{-2}	5.47×10^{-1}
kernel ridge reg		8.60×10^{-3}	2.38×10^{-3}	8.10×10^{-1}	1.24×10^{-1}	1.06×10^{-1}	6.30×10^0
neural net	Fourier	9.07×10^{-3} ($\lambda = 1 \times 10^{-2}$)	4.46×10^{-4} ($\lambda = 1 \times 10^{-4}$)	3.41×10^{-1} ($\lambda = 1 \times 10^{-1}$)	6.97×10^{-2} ($\lambda = 1 \times 10^{-1}$)	2.51×10^{-2} ($\lambda = 1 \times 10^{-3}$)	6.01×10^{-1} ($\lambda = 1 \times 10^{-1}$)
	sigmoid	9.21×10^{-3} ($\lambda = 0$)	1.67×10^{-4} ($\lambda = 1 \times 10^{-4}$)	3.31×10^{-1} ($\lambda = 1 \times 10^{-1}$)	8.01×10^{-2} ($\lambda = 1 \times 10^{-1}$)	7.86×10^{-2} ($\lambda = 1 \times 10^{-3}$)	1.57×10^0 ($\lambda = 1 \times 10^{-3}$)
	ReLU	5.92×10^{-4} ($\lambda = 1 \times 10^{-3}$)	4.72×10^{-4} ($\lambda = 0$)	3.66×10^{-1} ($\lambda = 1 \times 10^{-1}$)	6.73×10^{-2} ($\lambda = 1 \times 10^{-1}$)	2.71×10^{-2} ($\lambda = 1 \times 10^{-2}$)	2.23×10^0 ($\lambda = 1 \times 10^0$)
F-Opt	Fourier	6.96×10^{-1} ($\lambda = 1 \times 10^{-3}$)	3.51×10^0 ($\lambda = 1 \times 10^{-1}$)	1.05×10^0 ($\lambda = 1 \times 10^{-4}$)	9.97×10^{-1} ($\lambda = 1 \times 10^{-1}$)	1.01×10^0 ($\lambda = 1 \times 10^{-1}$)	1.01×10^0 ($\lambda = 1 \times 10^0$)
	sigmoid	1.57×10^{-2} ($\lambda = 1 \times 10^{-4}$)	1.91×10^{-4} ($\lambda = 0$)	5.92×10^{-1} ($\lambda = 1 \times 10^{-3}$)	7.35×10^{-2} ($\lambda = 1 \times 10^{-1}$)	7.38×10^{-2} ($\lambda = 1 \times 10^{-3}$)	5.79×10^{-1} ($\lambda = 1 \times 10^0$)
GFT	Fourier	8.31×10^{-7} ($\lambda = 0$)	3.31×10^{-5} ($\lambda = 0$)	2.34×10^{-1} ($\lambda = 1 \times 10^{-1}$)	8.06×10^{-2} ($\lambda = 1 \times 10^{-2}$)	1.05×10^{-2} ($\lambda = 1 \times 10^{-2}$)	5.66×10^{-1} ($\lambda = 1 \times 10^0$)
	sigmoid	1.22×10^{-5} ($\lambda = 0$)	7.42×10^{-5} ($\lambda = 0$)	2.90×10^{-1} ($\lambda = 1 \times 10^{-1}$)	6.86×10^{-2} ($\lambda = 1 \times 10^{-1}$)	1.35×10^{-2} ($\lambda = 1 \times 10^{-4}$)	9.68×10^{-1} ($\lambda = 1 \times 10^{-1}$)
GFT-r	Fourier	6.97×10^{-7} ($\lambda = 0$)	5.36×10^{-6} ($\lambda = 0$)	2.34×10^{-1} ($\lambda = 1 \times 10^{-1}$)	8.04×10^{-2} ($\lambda = 1 \times 10^{-2}$)	6.48×10^{-3} ($\lambda = 0 \times 10^0$)	5.65×10^{-1} ($\lambda = 1 \times 10^0$)
	sigmoid	1.67×10^{-5} ($\lambda = 0$)	1.85×10^{-5} ($\lambda = 0$)	2.89×10^{-1} ($\lambda = 1 \times 10^{-1}$)	6.84×10^{-2} ($\lambda = 1 \times 10^{-1}$)	9.39×10^{-3} ($\lambda = 0$)	9.88×10^{-1} ($\lambda = 1 \times 10^{-1}$)

implicit regularization. Incorporating similar sparsity constraints into our generative training is left for future research. Even without such a regularization, GFT-r achieves the best performance on most datasets. Again, both GFT and GFT-r achieve significantly better results than standard training with the Adam optimizer.

5 Discussion

Summary We proposed a training procedure for $f_{w,b}$ as in (1) with only a few hidden neurons w . In our procedure, we sample the w from a generative model and compute the optimal b by solving a linear system. To enhance the results, we apply a feature refinement scheme in the latent space of the generative model and regularize the loss function. Numerical examples have shown that the proposed generative feature training significantly outperforms standard training procedures.

Outlook Our approach can be extended in several directions. First, we want to train deeper networks in a greedy way similar to (Belilovsky et al., 2019). Recently, a similar approach was considered in the context of sampled networks by Bolager et al. (2023). Moreover, we can encode a sparse structure on the features by replacing the latent distribution $N(0, I_d)$ with a lower-dimensional latent model or by considering mixtures of generative models. From a theoretical side, we want to characterize the global minimizers of the functional in (8) and their relations to the Fourier transform of the target function.

Limitations If N in (1) gets large, solving the linear system (6) becomes expensive. However, this corresponds to the overparameterized regime where gradient-based methods work well. Moreover, the computation of the optimal b depends on all data points. Consequently, if we do minibatching, the output weights b are batch-dependent, and both the theoretical and practical implications remain open. Instead, we emphasize that one motivation for our method is the treatment of small data sets, where no minibatching is required. This is actually also one of the main use cases for 2-layer neural networks. Finally, note that GFT is currently restricted to the L_2 -loss function, which limits the applicability of GFT to non-regression tasks. For other loss functions, bilevel learning methods could be used to compute and differentiate the optimal output layer. This is beyond the scope of this paper, and we leave this point for future work.

Acknowledgments

We would like to thank Daniel Potts, Gabriele Steidl and Laura Weidensager for fruitful discussions. JH acknowledges funding by the German Research Foundation (DFG) within the Walter Benjamin Programme with project number 530824055 and by the EPSRC programme grant “The Mathematics of Deep Learning” with reference EP/V026259/1.

References

Robert Acar and Curtis R Vogel. Analysis of bounded variation penalty methods for ill-posed problems. *Inverse Problems*, 10(6):1217–1229, 1994.

Luigi Ambrosio, Nicola Fusco, and Diego Pallara. *Functions of Bounded Variation and Free Discontinuity Problems*. Oxford Mathematical Monographs. Oxford University Press, New York, 2000.

Fatima Antarou Ba, Oleh Melnyk, Christian Wald, and Gabriele Steidl. Sparse additive function decompositions facing basis transforms. *Foundations of Data Science*, 6(4):514–552, 2024.

Yatong Bai, Tanmay Gautam, and Somayeh Sojoudi. Efficient global optimization of two-layer ReLU networks: Quadratic-time algorithms and adversarial training. *SIAM Journal on Mathematics of Data Science*, 5(2):446–474, 2023.

Yaxuan Bai, Xiaofan Lu, and Linan Zhang. Function approximations via ℓ_1 - ℓ_2 optimization. *Journal of Applied & Numerical Optimization*, 6(3):371–389, 2024.

Adrian Barbu. Training a two-layer ReLU network analytically. *Sensors*, 23(8):4072, 2023.

Eugene Belilovsky, Michael Eickenberg, and Edouard Oyallon. Greedy layerwise learning can scale to ImageNet. In *International Conference on Machine Learning*, pp. 583–593. PMLR, 2019.

Charles Blundell, Julien Cornebise, Koray Kavukcuoglu, and Daan Wierstra. Weight uncertainty in neural network. In *International Conference on Machine Learning*, pp. 1613–1622. PMLR, 2015.

Erik Lien Bolager, Iryna Burak, Chinmay Datar, Qing Sun, and Felix Dietrich. Sampling weights of deep neural networks. In *Advances in Neural Information Processing Systems*, volume 37, 2023.

Digvijay Boob, Santanu S Dey, and Guanghui Lan. Complexity of training ReLU neural network. *Discrete Optimization*, 44:100620, 2022.

Tony F Chan and Selim Esedoglu. Aspects of total variation regularized l^1 function approximation. *SIAM Journal on Applied Mathematics*, 65(5):1817–1837, 2005.

Corinna Cortes, Mehryar Mohri, and Ameet Talwalkar. On the impact of kernel approximation on learning accuracy. In *International Conference on Artificial Intelligence and Statistics*, pp. 113–120, 2010.

Nello Cristianini and John Shawe-Taylor. *An introduction to support vector machines and other kernel-based learning methods*. Cambridge University Press, 2000.

Oliver RA Dunbar, Nicholas H Nelsen, and Maya Mutic. Hyperparameter optimization for randomized algorithms: a case study on random features. *Statistics and Computing*, 35(3):1–28, 2025.

Alok Dutt and Vladimir Rokhlin. Fast Fourier transforms for nonequispaced data. *SIAM Journal on Scientific Computing*, 14(6):1368–1393, 1993.

Weinan E, Chao Ma, and Lei Wu. A priori estimates of the population risk for two-layer neural networks. *Communications in Mathematical Sciences*, 17(5):1407–1425, 2019.

Alex Graves. Practical variational inference for neural networks. In *Advances in Neural Information Processing Systems*, volume 24, 2011.

Abolfazl Hashemi, Hayden Schaeffer, Robert Shi, Ufuk Topcu, Giang Tran, and Rachel Ward. Generalization bounds for sparse random feature expansions. *Applied and Computational Harmonic Analysis*, 62:310–330, 2023.

Johannes Hertrich. Fast kernel summation in high dimensions via slicing and Fourier transforms. *SIAM Journal on Mathematics of Data Science*, 6:1109–1137, 2024.

Johannes Hertrich, Tim Jahn, and Michael Quellmalz. Fast summation of radial kernels via QMC slicing. *International Conference on Learning Representations*, 2025.

David Holzmüller and Ingo Steinwart. Training two-layer ReLU networks with gradient descent is inconsistent. *Journal of Machine Learning Research*, 23(181):1–82, 2022.

Guang-Bin Huang, Qin-Yu Zhu, and Chee-Kheong Siew. Extreme learning machine: theory and applications. *Neurocomputing*, 70(1-3):489–501, 2006.

Laurent Valentin Jospin, Hamid Laga, Farid Boussaid, Wray Buntine, and Mohammed Bennamoun. Hands-on Bayesian neural networks—a tutorial for deep learning users. *IEEE Computational Intelligence Magazine*, 17(2):29–48, 2022.

Aku Kammonen, Jonas Kiessling, Petr Plecháč, Mattias Sandberg, and Anders Szepessy. Adaptive random Fourier features with Metropolis sampling. *Foundations of Data Science*, 2(3):309–332, 2020.

Kirthevasan Kandasamy and Yaoliang Yu. Additive approximations in high dimensional nonparametric regression via the SALSA. In *International Conference on Machine Learning*, pp. 69–78. PMLR, 2016.

Markelle Kelly, Rachel Longjohn, and Kolby Nottingham. The UCI machine learning repository, 2023. URL <https://archive.ics.uci.edu>.

Chun-Liang Li, Wei-Cheng Chang, Youssef Mroueh, Yiming Yang, and Barnabas Poczos. Implicit kernel learning. In *International Conference on Artificial Intelligence and Statistics*, pp. 2007–2016. PMLR, 2019a.

Lingfeng Li, Xue-Cheng Tai, and Jiang Yang. Generalization error analysis of neural networks with gradient based regularization. *Communications in Computational Physics*, 32(4):1007–1038, 2022.

Yang Li, Si Si, Gang Li, Cho-Jui Hsieh, and Samy Bengio. Learnable Fourier features for multi-dimensional spatial positional encoding. *Advances in Neural Information Processing Systems*, 34:15816–15829, 2021.

Yanjun Li, Kai Zhang, Jun Wang, and Sanjiv Kumar. Learning adaptive random features. In *Proceedings of the AAAI Conference on Artificial Intelligence*, volume 33, pp. 4229–4236, 2019b.

Zhu Li, Jean-Francois Ton, Dino Oglic, and Dino Sejdinovic. Towards a unified analysis of random Fourier features. In *International Conference on Machine Learning*, pp. 3905–3914. PMLR, 2019c.

Fanghui Liu, Xiaolin Huang, Yudong Chen, and Johan AK Suykens. Random features for kernel approximation: A survey on algorithms, theory, and beyond. *IEEE Transactions on Pattern Analysis and Machine Intelligence*, 44(10):7128–7148, 2021.

Aaron Mishkin, Arda Sahiner, and Mert Pilanci. Fast convex optimization for two-layer ReLU networks: Equivalent model classes and cone decompositions. In *International Conference on Machine Learning*, pp. 15770–15816. PMLR, 2022.

Radford M Neal. *Bayesian Learning for Neural Networks*. Springer Science & Business Media, 2012.

Mert Pilanci and Tolga Ergen. Neural networks are convex regularizers: Exact polynomial-time convex optimization formulations for two-layer networks. In *International Conference on Machine Learning*, pp. 7695–7705. PMLR, 2020.

Daniel Potts and Michael Schmischke. Interpretable approximation of high-dimensional data. *SIAM Journal on Mathematics of Data Science*, 3(4):1301–1323, 2021.

Table 4: Comparison for function approximation with: We report the MSE over the test set averaged over 5 runs. The table contains the same experiments as Table 1 with $N = 50$ features. The deployed λ is indicated below each result. The best performance is highlighted.

Method		Function f_1		Function f_2		Function f_3	
Method	Activation	$(d, M) = (5, 300)$	$(d, M) = (10, 500)$	$(d, M) = (5, 500)$	$(d, M) = (10, 1000)$	$(d, M) = (5, 500)$	$(d, M) = (10, 200)$
neural net	Fourier	3.35×10^{-5} ($\lambda = 0$)	9.22×10^{-5} ($\lambda = 1 \times 10^{-4}$)	6.97×10^{-6} ($\lambda = 0$)	8.15×10^{-6} ($\lambda = 0$)	2.45×10^{-3} ($\lambda = 1 \times 10^{-4}$)	4.65×10^0 ($\lambda = 1 \times 10^{-3}$)
	sigmoid	1.03×10^{-5} ($\lambda = 0$)	1.52×10^{-5} ($\lambda = 0$)	1.19×10^{-5} ($\lambda = 0$)	1.45×10^{-5} ($\lambda = 1 \times 10^{-4}$)	2.14×10^{-3} ($\lambda = 0$)	2.27×10^0 ($\lambda = 1 \times 10^{-4}$)
F-Opt	ReLU	4.71×10^{-4} ($\lambda = 0$)	1.40×10^{-3} ($\lambda = 0$)	3.00×10^{-4} ($\lambda = 0$)	1.12×10^{-4} ($\lambda = 1 \times 10^{-4}$)	2.08×10^{-1} ($\lambda = 0$)	1.89×10^0 ($\lambda = 1 \times 10^{-4}$)
	Fourier	1.60×10^{-5} ($\lambda = 1 \times 10^{-4}$)	2.52×10^0 ($\lambda = 0$)	5.01×10^{-6} ($\lambda = 0$)	7.45×10^0 ($\lambda = 0$)	5.13×10^{-3} ($\lambda = 1 \times 10^{-4}$)	2.60×10^2 ($\lambda = 1 \times 10^{-4}$)
GFT	sigmoid	2.44×10^{-4} ($\lambda = 0$)	8.05×10^{-5} ($\lambda = 1 \times 10^{-4}$)	3.58×10^{-3} ($\lambda = 1 \times 10^{-4}$)	1.69×10^{-6} ($\lambda = 0$)	1.08×10^0 ($\lambda = 1 \times 10^{-4}$)	3.94×10^0 ($\lambda = 1 \times 10^{-4}$)
	Fourier	9.49×10^{-5} ($\lambda = 0$)	4.19×10^{-5} ($\lambda = 1 \times 10^{-3}$)	5.71×10^{-5} ($\lambda = 1 \times 10^{-3}$)	1.98×10^{-5} ($\lambda = 1 \times 10^{-4}$)	9.17×10^{-2} ($\lambda = 1 \times 10^{-3}$)	8.72×10^{-3} ($\lambda = 1 \times 10^{-4}$)
GFT-r	sigmoid	1.94×10^{-1} ($\lambda = 1 \times 10^{-4}$)	6.08×10^{-5} ($\lambda = 1 \times 10^{-3}$)	5.41×10^{-1} ($\lambda = 1 \times 10^{-4}$)	9.01×10^{-4} ($\lambda = 1 \times 10^{-2}$)	9.81×10^0 ($\lambda = 1 \times 10^{-4}$)	1.09×10^{-2} ($\lambda = 0$)
	Fourier	5.52×10^{-6} ($\lambda = 0$)	2.94×10^{-7} ($\lambda = 0$)	1.24×10^{-6} ($\lambda = 0$)	9.75×10^{-7} ($\lambda = 1 \times 10^{-4}$)	8.72×10^{-3} ($\lambda = 0$)	2.02×10^{-4} ($\lambda = 0$)
	sigmoid	1.94×10^{-1} ($\lambda = 1 \times 10^{-4}$)	6.96×10^{-2} ($\lambda = 0$)	4.33×10^{-1} ($\lambda = 0$)	4.78×10^{-1} ($\lambda = 1 \times 10^{-4}$)	2.66×10^0 ($\lambda = 0$)	2.82×10^{-3} ($\lambda = 0$)

Daniel Potts and Laura Weidensager. ANOVA-boosting for random Fourier features. *Applied and Computational Harmonic Analysis*, 79:101789, 2025.

Daniel Potts, Gabriele Steidl, and Manfred Tasche. Fast Fourier transforms for nonequispaced data: A tutorial. *Modern Sampling Theory: Mathematics and Applications*, pp. 247–270, 2001.

Ali Rahimi and Benjamin Recht. Random features for large-scale kernel machines. In *Advances in Neural Information Processing Systems*, volume 20, 2007.

Ali Rahimi and Benjamin Recht. Uniform approximation of functions with random bases. In *46th Annual Allerton Conference on Communication, Control, and Computing*, pp. 555–561. IEEE, 2008.

Alessandro Rudi and Lorenzo Rosasco. Generalization properties of learning with random features. In *Advances in Neural Information Processing Systems*, volume 30, 2017.

Nicolaj Rux, Michael Quellmalz, and Gabriele Steidl. Slicing of radial functions: a dimension walk in the Fourier space. *Sampling Theory, Signal Processing, and Data Analysis*, 23(1):1–40, 2025.

Esha Saha, Hayden Schaeffer, and Giang Tran. HARFE: Hard-ridge random feature expansion. *Sampling Theory, Signal Processing, and Data Analysis*, 21(2):27, 2023.

Yuege Xie, Robert Shi, Hayden Schaeffer, and Rachel Ward. SHRIMP: Sparser random feature models via iterative magnitude pruning. In *Proceedings of Mathematical and Scientific Machine Learning*, volume 190, pp. 303–318. PMLR, 2022.

Ian En-Hsu Yen, Ting-Wei Lin, Shou-De Lin, Pradeep K Ravikumar, and Inderjit S Dhillon. Sparse random feature algorithm as coordinate descent in Hilbert space. In *Advances in Neural Information Processing Systems*, volume 27, 2014.

A Dependence on the Number of Features

We redo the experiments from Section 4.3 for $N = 50$ and $N = 200$. The results are given in Table 4 and 5.

Table 5: Comparison for function approximation with: We report the MSE over the test set averaged over 5 runs. The table contains the same experiments as Table 1 with $N = 200$ features. The deployed λ is indicated below each result. The best performance is highlighted.

Method		Function f_1		Function f_2		Function f_3	
Method	Activation	$(d, M) = (5, 300)$	$(d, M) = (10, 500)$	$(d, M) = (5, 500)$	$(d, M) = (10, 1000)$	$(d, M) = (5, 500)$	$(d, M) = (10, 200)$
neural net	Fourier	7.22×10^{-4} ($\lambda = 0$)	1.21×10^{-2} ($\lambda = 1 \times 10^{-4}$)	1.56×10^{-4} ($\lambda = 1 \times 10^{-4}$)	1.36×10^{-4} ($\lambda = 1 \times 10^{-4}$)	2.26×10^{-3} ($\lambda = 1 \times 10^{-4}$)	3.95×10^0 ($\lambda = 0$)
	sigmoid	1.54×10^{-5} ($\lambda = 0$)	2.35×10^{-5} ($\lambda = 0$)	1.46×10^{-5} ($\lambda = 1 \times 10^{-4}$)	4.91×10^{-5} ($\lambda = 0$)	1.21×10^{-3} ($\lambda = 1 \times 10^{-4}$)	1.79×10^0 ($\lambda = 0$)
F-Opt	ReLU	3.03×10^{-4} ($\lambda = 0$)	1.05×10^{-3} ($\lambda = 0$)	1.78×10^{-4} ($\lambda = 0$)	2.02×10^{-4} ($\lambda = 1 \times 10^{-4}$)	6.20×10^{-2} ($\lambda = 1 \times 10^{-4}$)	1.84×10^0 ($\lambda = 1 \times 10^{-4}$)
	Fourier	9.45×10^{-3} ($\lambda = 1 \times 10^{-3}$)	1.52×10^{-2} ($\lambda = 1 \times 10^{-2}$)	4.47×10^{-5} ($\lambda = 1 \times 10^{-4}$)	2.34×10^{-2} ($\lambda = 1 \times 10^{-2}$)	1.29×10^0 ($\lambda = 1 \times 10^{-2}$)	2.11×10^1 ($\lambda = 1 \times 10^0$)
GFT	sigmoid	2.32×10^{-6} ($\lambda = 0$)	5.73×10^{-4} ($\lambda = 1 \times 10^{-4}$)	1.19×10^{-6} ($\lambda = 0$)	8.92×10^{-5} ($\lambda = 0$)	7.23×10^{-4} ($\lambda = 0$)	2.40×10^0 ($\lambda = 0$)
	Fourier	6.66×10^{-7} ($\lambda = 0$)	2.33×10^{-7} ($\lambda = 0$)	5.73×10^{-8} ($\lambda = 0$)	6.53×10^{-7} ($\lambda = 0$)	2.26×10^{-5} ($\lambda = 0$)	1.51×10^0 ($\lambda = 1 \times 10^{-4}$)
GFT-r	sigmoid	2.84×10^{-6} ($\lambda = 0$)	3.52×10^{-6} ($\lambda = 0$)	2.04×10^{-7} ($\lambda = 0$)	3.05×10^{-7} ($\lambda = 0$)	1.62×10^{-4} ($\lambda = 0$)	1.75×10^{-2} ($\lambda = 0$)
	Fourier	1.57×10^{-7} ($\lambda = 0$)	6.01×10^{-8} ($\lambda = 0$)	1.42×10^{-8} ($\lambda = 0$)	1.66×10^{-7} ($\lambda = 0$)	1.28×10^{-6} ($\lambda = 0$)	1.82×10^0 ($\lambda = 1 \times 10^{-4}$)
	sigmoid	2.04×10^{-6} ($\lambda = 0$)	2.26×10^{-6} ($\lambda = 0$)	4.27×10^{-8} ($\lambda = 0$)	5.41×10^{-8} ($\lambda = 0$)	1.84×10^{-5} ($\lambda = 0$)	1.60×10^{-2} ($\lambda = 0$)

Table 6: Comparison for function approximation with: We report the MSE over the test set averaged over 5 runs. The table contains the same experiments as Table 1 for the two ablations in Appendix B. The deployed λ is indicated below each result.

Method		Function f_1		Function f_2		Function f_3	
Method	Activation	$(d, M) = (5, 300)$	$(d, M) = (10, 500)$	$(d, M) = (5, 500)$	$(d, M) = (10, 1000)$	$(d, M) = (5, 500)$	$(d, M) = (10, 200)$
Fully Sampled	Fourier	1.41×10^{-3} ($\lambda = 1 \times 10^{-4}$)	1.55×10^{-2} ($\lambda = 1 \times 10^{-3}$)	4.01×10^{-2} ($\lambda = 1 \times 10^{-3}$)	3.73×10^{-2} ($\lambda = 1 \times 10^{-4}$)	4.89×10^0 ($\lambda = 0$)	5.70×10^0 ($\lambda = 1 \times 10^{-1}$)
Noisy gradients	Fourier	1.03×10^{-2} ($\lambda = 0$)	7.56×10^{-3} ($\lambda = 1 \times 10^{-2}$)	7.04×10^{-3} ($\lambda = 0$)	4.16×10^{-3} ($\lambda = 1 \times 10^{-2}$)	1.38×10^{-2} ($\lambda = 1 \times 10^{-4}$)	7.83×10^0 ($\lambda = 1 \times 10^{-4}$)

B Further Ablations

First, to demonstrate that using the optimal output weights $b(w)$ from Section 3.1 is necessary for GFT, we run the following experiment: Instead of sampling only features w_l from a generative model $p_w = G_{\theta \# \eta}$ with $G_{\theta}: \mathbb{R}^d \rightarrow \mathbb{R}^d$ and then computing $b(w)$, we sample pairs (w_l, b_l) from $p_{w,b} = \tilde{G}_{\theta \# \tilde{\eta}}$ for $\tilde{G}_{\theta}: \mathbb{R}^{d+2} \rightarrow \mathbb{R}^d \times \mathbb{C}$ and the $d+2$ dimensional standard normal distribution $\tilde{\eta}$. We use the Fourier activation and the same setup as for Table 1. The results in the first row of Table 6 are significantly worse than for GFT and GFT-r in Table 1. This is not surprising since now each output weight b_l only depends on its corresponding feature w_l instead of all $(w_l)_{l=1}^N$ as for the optimal $b(w)$. In particular, $b(w)$ cannot be learned by a gradient-based algorithms since in each update the $w = (w_l)_{l=1}^N$ are resampled. Thus, there is no persisting correspondence of sampled features with specific output weights.

Second, we test whether the neural network line in Table 1 can be improved by introducing gradient noise. This technique can help to escape local minima. To this end, we optimize the same loss function as for the 2-layer neural network in Table 1, but use the noisy stochastic gradient descent $\theta_{n+1} = \theta_n - \rho \nabla L(\theta) + \alpha Z$ with random $Z \sim \mathcal{N}(0, I)$, step size ρ , and noise strength $\alpha = 0.1\rho$. The obtained results in the second row of Table 6 do not improve upon the baseline from Table 1.

C Implementation Details

We optimize the loss functions for GFT and for the feature refinement with the Adam optimizer using a learning rate of 1×10^{-4} for 40000 steps. The regularization ϵ for solving the least squares problem (6) is

set to $\epsilon = 1 \times 10^{-7}$. For the neural network optimization, we use the Adam optimizer with a learning rate of 1×10^{-3} for 100000 steps. In all cases, we discretize the spatial integral for the regularization term in (10) by 1000 samples. For the kernel ridge regression, we use a Gauss kernel with its parameter chosen by the median rule. That is, we set it to the median distance of two points in the dataset. The PyTorch implementation corresponding to our experiments is available at https://github.com/johertrich/generative_feature_training.